



ELSEVIER

Earth and Planetary Science Letters 164 (1998) 205–219

EPSL

Large-scale crustal heterogeneities and lithospheric strength in cratons

E. Burov^a, C. Jaupart^{b,*}, J.C. Mareschal^c

^a Bureau de Recherches Géologiques et Minières, B.P. 6009, Orléans Cedex 2, France

^b Institut de Physique du Globe de Paris, Pl. Jussieu, F-75252, Paris Cedex 5, France

^c GEOTOP, Centre de Recherche en Géochimie Isotopique et en Géochronologie, Université du Québec à Montréal, C.P. 8888, succ. 'Centre-Ville', Montreal, H3C3P8, Canada

Received 16 January 1998; revised version received 17 July 1998; accepted 30 July 1998

Abstract

The rheology and thermal structure of the continental lithosphere are intimately linked. In old cratons, the effective elastic thickness of the lithosphere has been estimated by various spectral (inverse) methods based on the correlation between topography and gravity anomalies. Estimates vary within a very large range from ≈ 40 km to 120 km depending on the method used. In this paper, we use forward models to account for lateral variations in mechanical properties and their effect on the equivalent elastic thickness (EET) of the lithosphere. From these models, which allow brittle–elastic–ductile rheologies and mechanical discontinuities (faults), we have calculated the strain/stress distributions and displacement fields. Vertical integration of the stress permits a local determination of the effective elastic thickness. The computed displacements were used to calculate related Bouguer and free-air gravity anomalies and compare them with the observations. The analysis is applied to the 2000-Ma Kapuskasing uplift (in the Superior Province of the Canadian Shield) where the presence of a high-density block in the upper crust is due to the upthrusting of midcrustal rocks along a major thrust fault. The study shows that the stability of this structure on geologic time scales requires a strong lower crustal rheology, a cold geotherm, and the fault to be healed. This study also shows that, because of stress dependence of the non-linear rheology, crustal heterogeneities may cause significant ($\approx 40\%$) local reductions of the lithospheric strength. Away from the Kapuskasing structure, the average strength of the lithosphere remains high (EET ≈ 100 km). Conventional methods for estimating the elastic thickness would not resolve such local strength reductions in cratons, but would predict, depending on the method used, highly overestimated or instead, underestimated EET. © 1998 Elsevier Science B.V. All rights reserved.

Keywords: cratons; stress; strain; Kapuskasing Zone; lithosphere

1. Introduction

Gravity studies of the elastic response of the continental lithosphere beneath the cratons predicted large values of lithospheric strength which is measured in terms of the effective elastic thickness (EET)

[1–5]. Cratonic areas are characterized by generally low topography and a complicated geological structure. On closer examination, it appears that anomalous values of the EET (very high or very low) frequently correspond to areas where data quality is poor. For example, in Africa, these anomalous values are systematically found in regions with lowest data density [5]. In the Canadian Shield, large values

* Corresponding author. E-mail: cj@ipgp.jussieu.fr

of the elastic thickness are found in regions with low-amplitude topography variations where the associated Bouguer gravity anomalies tend to be small (≈ 10 mGal). Thus, the signal-to-noise ratio is bad and the anomalies associated with the lithospheric deformation are on the order of the accuracy of the data (few mGal from most gridded data sets). Similar limitations also apply to the spectral methods (admittance) based on much shorter-wavelength free-air gravity anomalies [6] which yield lower estimates of EET. Recently, spectral analysis based on the maximum entropy method was used to improve the spatial resolution of the data [7]. The coherence method has also been modified to account for the effect of internal loads correlated with the topography [8].

All the spectral methods assume that the gravity signal results from the static deflection of a continuous thin plate (with constant elastic moduli) under loading by the surface topography or subsurface loads. Boundary forces and lithospheric discontinuities are neglected. It is thus difficult to interpret the gravity-based EET estimates in cratons where the loads are largely internal, i.e. within the crust, and correspond to specific geological structures [9]. Large values of the elastic thickness require long-wavelength data, i.e. over wide areas encompassing several geological provinces. In such conditions, internal loads correspond to different crustal blocks with varying mechanical properties. Consequently, it is not proper to assume loads distributed on and within a mechanically homogeneous elastic plate. In other words, for old continental regions, deformation in a structure with complex rheological variations cannot be characterized by a single parameter.

Because of inconsistencies between the previous results, it is useful to take an alternative approach. In this paper, we use 2D forward mechanical models that account for internal loads, boundary forces, and mechanical discontinuities. At the same time, we use the method of estimating the EET developed in [10]. This method is based on the definition of EET used in the theory of thin plates and shells. To treat the beams and plates of a finite thickness, the thin plate theory imposes strict relations between the stress–strain depth distribution, elastic properties and the derivatives of the plate deflection. The local bending moments and fibre forces are expressed via depth integrals of stress and strain. With the flexural

term expressed through the bending moment, the thin plate equations are independent of the rheology and the EET of any plate can be derived directly from the relations between these moments and the elastic moduli of the plate.

The *observed* EET of the lithosphere is defined as the thickness of an imaginary elastic plate which would have the same deflection under applied tectonic loads as that of the real (inelastic) lithosphere. This definition uses the thin plate flexural equations with an unknown EET which is fitted to the *observed* plate deflection. Because the deflection of the continental lithosphere cannot be observed directly, it is derived from gravity modelling or seismic data. Theoretically, the *internal* EET obtained from the bending moments is equivalent to the *observed* EET derived from geophysical data. This is indeed verified in the oceans where EETs predicted from rheology and thermal structure match very well the observed values [11]. Such a good correlation has not been found in the continents. Any misfit can be due to the gravity model, or the rheology and thermal model. With sufficient data, the *observed* EET can be used to constrain the rheology and temperature model. For example, assumption of a weak (decoupled) lower crustal rheology would require EET values about 2 times lower than those for a strong lower crust [10]. Alternatively, the rheology-based EET can be used to verify the ‘observed’ values derived from the traditional models.

In this study, we shall analyze the effect of crustal heterogeneities on the EET near the Kapuskasing uplift, a large structural zone which cross-cuts Archaean belts of the Superior Province in the Canadian Shield.

2. The Kapuskasing structural zone

2.1. Geological and tectonic environment

The Kapuskasing structural zone (KSZ) cuts obliquely the predominantly E–W structures of the Superior Province in the Canadian Shield: the Abitibi–Wawa granite–greenstone belts to the south, and the Quetico–Opatica metasedimentary belts to the north (Fig. 1). Different workers interpreted this structure either as a suture, transcurrent shear zone or

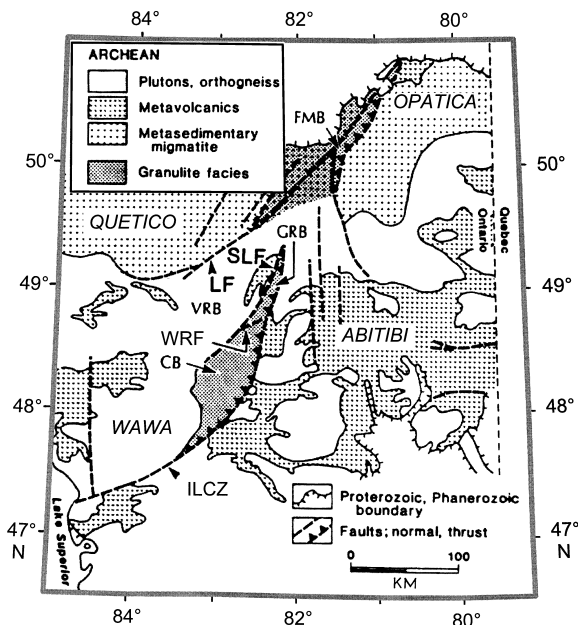


Fig. 1. Geo-tectonic sketch of the Kapuskasing structural zone (after [12]): LF = Lepage fault, SLF = Saganash Lake fault, WRF = Wakusimi River fault, ILCZ = Ivanhoe Lake Cataclastic Zone, FMB = Fraserdale–Moosonee Block, GRB = Groundhog River Block, CB = Chapleau Block, VRB = Val-Rita Block.

intra-cratonic thrust [13]; the latter hypothesis seems supported by the most recent data.

Across the southern segment of the KSZ, geobarometric studies show a continuous transition from low-grade greenstones in the Michipicoten belt, to amphibolite facies tonalite in the Wawa gneiss terrane, to high-grade granulite-facies rocks in the KSZ [14]. An abrupt return to low-grade conditions occurs across the Ivanhoe Lake Fault Zone (ILFZ) which marks the eastern limit of the KSZ. Percival and McGrath [15] have interpreted the KSZ as a slab of deep crust thrust along the ILFZ. Geological and geophysical studies, and the LITHOPROBE seismic transect have confirmed the thrust hypothesis, and have constrained the timing and mechanism of crustal shortening [13].

A variety of radiometric methods have been used to constrain the cooling and uplift history (see references in [13]). The crust in the Wawa and Abitibi belts stabilized at 2700–2650 Ma. Regional differences in radiometric ages for minerals with low closing temperature indicate that movement on the

ILFZ may have started as early as at 2500 Ma. However, the study of dike swarms [16] shows that the main uplift occurred in the Early Proterozoic (2000–1900 Ma), possibly because of compression along the western margin of the craton (Trans-Hudson orogen).

Seismic reflection data are consistent with the thrust model [14]. The westward dip of seismic reflectors in the Abitibi belt changes markedly beneath the ILFZ and a weak seismic reflector dipping at 45° could be the fault itself [17]. Seismic refraction data show a broad zone of the upper crust with higher than normal velocity that dips ≈20° to the northwest [12]. This region is also characterized by higher values of Poisson's ratio in the upper crust and a regional increase in crustal thickness from ≈44 km to >52 km just west of the ILFZ [18,19]. Crustal thickness decreases to ≈40 km in the Abitibi subprovince to the east. Wu and Mereu [20] have argued that the Moho is not very well defined and that uniform crustal thickness across the KSZ cannot be ruled out by the available seismic data. However, gravity data do support the existence of a thicker crust [21]. Various estimates have been proposed for the amount of shortening. Boland and Ellis [12] assumed that the dip of the thrust fault is the same as that of the reflectors imaged under the ILFZ (≈20°) and obtained 50–80 km of shortening. Percival and West [13] suggested a much steeper fault coinciding with a weak reflector and an offset of strong reflectors on both sides of the ILFZ. They found that dextral transpression along a 35°-west-dipping ILFZ resulted in 27 km total shortening. All these authors assume that the fault soles to a horizontal decollement at mid-crustal depth and that brittle deformation in the upper crust was accompanied by ductile flow in the lower crust.

2.2. Gravity and flexure

The KSZ is barely seen on topographic maps (undulations of 200–300 m), but it is well marked in the gravity anomaly, where it has a signature similar to that of a narrow mountain belt. The positive Bouguer anomaly associated with the KSZ (Fig. 2) has been explained by the presence of dense granulite-facies rocks brought upwards along a west-dipping thrust. This anomaly has no corresponding topographic ex-

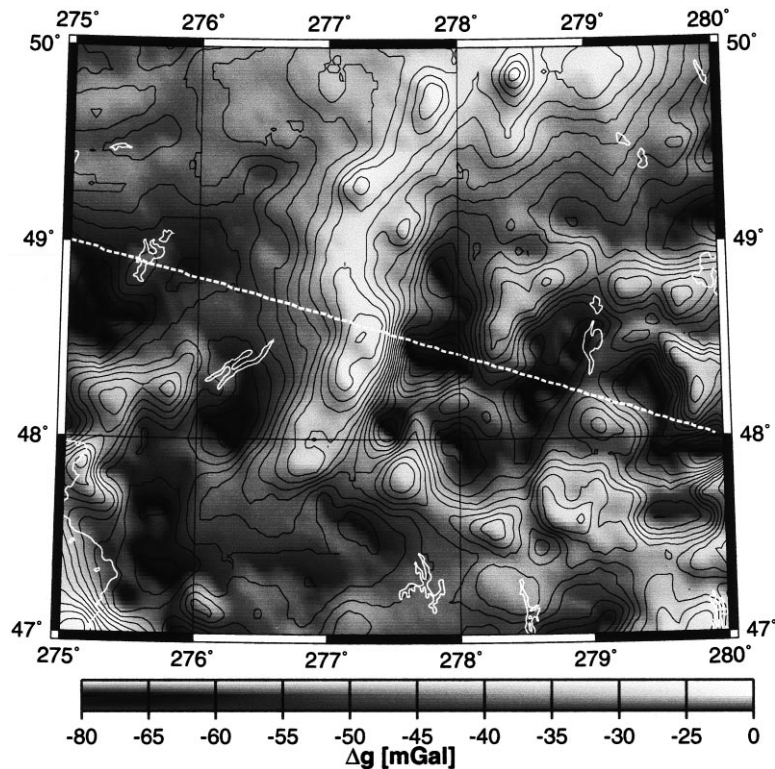


Fig. 2. Bouguer gravity map for the Kapuskasing uplift area. The spatial resolution is $2.5' \times 2.5'$. The profile analyzed in Fig. 3 is marked by the discontinuous line.

pression, but there is a long-wavelength topography gradient of small amplitude (Fig. 3). The Bouguer gravity profile is also characterized by short-wavelength small-amplitude fluctuations induced by shallow sources (mostly plutons). For the present study, we shall neglect these features and focus on the Kapuskasing structure. The Bouguer anomaly increases from about -50 mGal, 200 km west of the ILFZ, to 0 mGal just west of the fault. East of the fault, the Bouguer anomaly decreases over a short distance.

In the Airy isostatic model with uniform crustal density, the topography should correlate with a long-wavelength eastward increase in Bouguer anomaly which is not observed (Fig. 3). Calculations of regional compensation with two different elastic plate thicknesses, 50 and 100 km, yield results far from the observed values (Fig. 3). The combination of long- and short-wavelength variations is impossible to reproduce with a uniform plate. In conventional admittance methods [1,2], the poor correlation between gravity and topography implies that the plate

is very thick. On the other hand, the free-air anomaly data show a good correlation with the short-wavelength topography and would lead to a small elastic thickness value.

The episode of transpressive faulting at ca. 1900 Ma was accompanied by crustal thickening [13]. The mechanism that permits the persistence of an uncompensated root over geologically long time scales is still debated [22]. Indeed, in the Airy isostatic limit, such a root would require a topography of about 2 km. For a much stronger lithosphere, as expected in a cratonic zone, the topography has to be even higher. If the previously existing topography was eroded away, the root should disappear through mantle flow in less than 50 m.y. (e.g. [23–25]). Without active tectonic processes, the persistence of the root requires a very strong rheology such as that of dry diabase or mafic granulites suggested in [22].

From the mechanical point of view, the presence of dense granulites in the upper crust provides an extra load on the mantle lithosphere and can induce

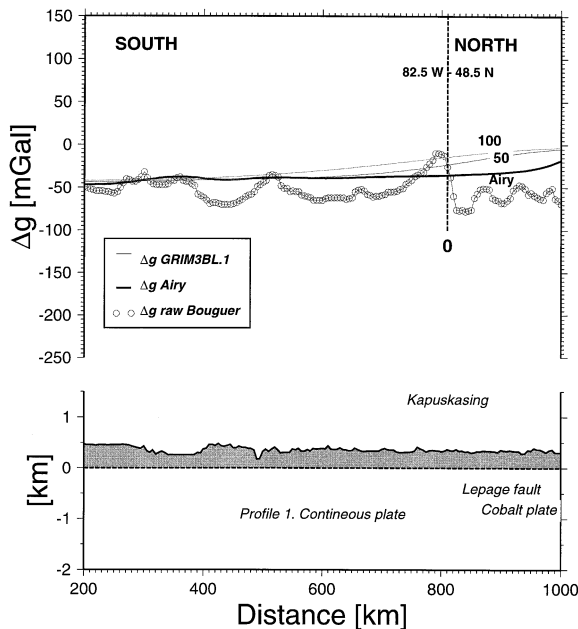


Fig. 3. Topographic and gravity profile across the uplift zone: predicted gravity anomalies for various classical homogeneous plate models with EET = 0 (solid curve), 50, and 100 km. The standard Bouguer anomaly calculated with density of 2670 kg m^{-3} was corrected to account for the higher average density (2750 kg m^{-3} circles) in the area.

Moho deflections not associated with the load of surface topography. The heterogeneous crustal structure and the mechanical discontinuity of the fault may result in a local reduction of the EET. In order to show that both effects significantly affect the EET estimates for the Kaspuskasing uplift, we shall use forward mechanical modelling that includes the brittle–elasto–ductile rheology and mechanical discontinuities associated with major faults.

2.3. Heat flow data

Determining the thermal structure and thickness of the lithosphere from heat flow data requires the knowledge of the distribution of radioactive elements within the crust. A systematic measurement program undertaken in the Canadian Shield has improved our understanding of the surface heat flow field and of the deep thermal structure [26–29]. These studies have concluded that the mantle heat flow beneath the Canadian Shield was $12 \pm 2 \text{ mW m}^{-2}$. For an average surface heat flow of 41 mW m^{-2} , it is possible to

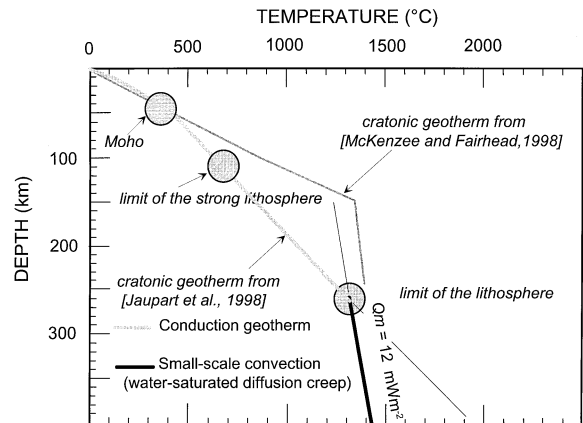


Fig. 4. Thermal model for the Canadian Shield based on heat flow data (after [30]).

calculate a conductive steady-state geotherm, regardless of the mechanism which fixes the base of the lithosphere [30]. One uncertainty is the poor knowledge of thermal conductivity at high temperatures. Using all available data on thermal conductivity (see references above), one can show that the geotherm is close to that calculated for a constant conductivity of $2.8\text{--}2.9 \text{ W m}^{-1} \text{ K}^{-1}$. This geotherm, shown in Fig. 4, yields a Moho temperature of 350°C (dashed line). Our working model for the Canadian Shield has the 700°C isotherm at a depth of about 120 km. Combined with the deformation models of [10], this thermal model is consistent with estimates of the effective elastic thickness in the area. We also use a ‘hot’ thermal model with a surface heat flow of 51 mW m^{-2} , for which the Moho temperature is 450°C , to investigate the behaviour of a weak lithosphere.

3. Mechanical model

3.1. Basic equations

The EET of a plate with arbitrary inelastic rheology can be calculated directly from the geometry of plate deformation and the rheological structure [10] (see Appendix A). The plate deformation is calculated by solving the conservation equations for energy, mass and momentum, together with bound-

ary conditions and constitutive equations for rocks:

$$\frac{\partial \rho}{\partial t} + \nabla \cdot \rho v = 0 \quad (1)$$

$$\nabla \cdot \sigma + \rho g = 0 \quad (2)$$

$$\rho C_p \frac{\partial T}{\partial t} + v \cdot \nabla T = \nabla(K \nabla T) + H \quad (3)$$

where v is velocity, ρ is density, T is temperature, g is the acceleration of gravity, σ is the stress tensor, C_p is the specific heat, K is the thermal conductivity, H is the (radiogenic and dissipative) heat generation.

3.2. Constitutive relations and material properties

The stress distribution is determined by the rheology of the rocks under the pressure, stress/strain and temperature conditions. For the plastic–elastic–viscous rheology used in our experiments, the strain rate $\dot{\epsilon}$, and the stress σ are related by a temperature-dependent power law viscosity: μ_{eff}

$$\dot{\epsilon} = \frac{\sigma}{2\mu_{\text{eff}}} \quad (4)$$

$$\dot{\epsilon} = \sigma^n A^* (-H^*/RT) \quad (5)$$

where A^* is a material constant, H^* is creep activation enthalpy, $R = 8.314 \text{ J mol}^{-1} \text{ K}^{-1}$ is the gas constant and T is thermodynamic temperature. The rheology and the parameters used are given in Table 1.

In the plastic part, the Mohr–Coulomb plasticity ($\sigma_t = \text{tg}(\beta)\sigma_n + \sigma_0$) with friction angle β of 30° and cohesion σ_0 of 20 MPa is used to approximate Byerlee's law [35] of brittle frictional failure:

$$\sigma_3 = (\sigma_1 - \sigma_3)/3.9; \quad \sigma_3 < 120 \text{ MPa} \quad (6)$$

$$\sigma_3 = (\sigma_1 - \sigma_3)/2.1 - 100; \quad \sigma_3 \geq 120 \text{ MPa} \quad (7)$$

where σ_1 and σ_3 are the minimum and maximum principal stresses. Additionally, weak strain softening is assumed as reduction of the cohesion to zero at strains larger than 0.1.

In the elastic part, standard values, $E = 0.8 \text{ GPa}$ and $\nu = 0.25$, were used for Young's modulus and Poisson's ratio [10].

Table 1

Parameters of dislocation creep for lithospheric rocks and minerals

Mineral/rock	A^* ($\text{Pa}^{-n} \text{ s}^{-1}$)	H^* (kJ mol^{-1})	n
Quartzite (dry)	5×10^{-12} 2.7×10^{-20}	190 156	3 2.4
Diorite (dry)	5×10^{-20} 5.2×10^{-18}	212 219	2.4 2.4
Diabase (dry)	6.3×10^{-20} 8.0×10^{-25}	276 260	3 3.4
Dunite (dry)	7×10^{-14}	520	3
Dislocation creep at $\sigma_1 - \sigma_3 < 200 \text{ MPa}$	2.5×10^{-17}	532	3.5
Dunite (dry)	$\dot{\epsilon} = \dot{\epsilon}_0 \exp \left[-\frac{H^*}{RT} \left(1 - \left(\frac{\sigma_1 - \sigma_3}{\sigma_0} \right)^2 \right) \right]$		
Dorn's creep	with $\dot{\epsilon}_0 = 5.7 \times 10^{-11} \text{ s}^{-1}$, $\sigma_0 = 8.5 \times 10^3 \text{ MPa}$, $H^* = 535 \text{ kJ mol}^{-1}$		

The values in the first lines correspond to the lower bounds on the rock strength [31,32]. The stronger values used in this study come from [33,34].

In order to study the effect of the ILFZ and the low-angle thrust beneath it, a simple classical Amonton's friction law on the fault was adopted:

$$\sigma_t = k\sigma_n \quad (8)$$

where σ_t , σ_n are the tangential and normal stress components on the fault surface, and k stands for the friction coefficient (between 0 and 1). At present, the 2-Ga-old fault is likely to be healed, implying that $k = 1$. Calculations were made with various k values in order to evaluate the effect of slip along the fault. The other material parameters are given in Tables 2 and 3.

Table 2

Density, conductivity and thermal diffusivity of the lithosphere

Layer	ρ (kg m^{-3})	K ($\text{W m}^{-1} \text{ K}^{-1}$)	κ ($\mu\text{m}^2 \text{ s}^{-1}$)
Upper crust	2.700	2.5	0.83
Lower crust	2.950	2	0.67
Mantle	3.300	3.5	0.88

Table 3
Thermal parameters used in the numerical models

Model	Surface heat flow (mW m ⁻²)	Moho temperature (°C)	Depth (700°C) (km)	Depth (1300°C) (km)
'hot'	51	450	82	170
'cold'	42	350	120	260

In the upper crust, heat production decreases exponentially with folding depth $D = 10$ km. It is 7.5×10^{-10} W kg⁻¹ at the surface. It is constant below 20 km.

3.3. Boundary conditions

On both vertical sides of the model, the horizontal velocity is fixed and pressure is assumed to be lithostatic. The Kapuskasing area experienced little horizontal compression, and the shortening may have taken place with a velocity as low as 1 mm y⁻¹, which was adopted as a boundary condition. This velocity yields background strain rates lower than 10⁻¹⁷ s⁻¹, which correspond to small stresses in the present framework. Winkler restoring forces are used at the base of the model. On the upper surface, it is assumed, following the common assumption of the flexural models, that any surface depression which occurs below the sea level is instantly filled with sediments that have the physical properties of the upper crust. For simplicity, erosion was not included in the present study.

We start the calculations with a given crustal load, for which mechanical equilibrium is not achieved. In reality, the load has been emplaced tectonically in a compressional regime involving significant far-field stresses. These effects are not included here because we are interested in the long-term response of the lithosphere. Thus, the initial transient evolution is not meant to be realistic.

3.4. Model geometry

As discussed above, the Kapuskasing structure has been interpreted as a low-angle thrust bringing deep crustal formations to the surface. The mechanical properties of the crust vary horizontally. Furthermore, there is a correlation between horizontal changes in mechanical properties and crustal density. In our model, the crust is made of two types of materials: quartz-dominated upper crustal rocks and diabase lower crustal rocks (Table 1). The thickness

of the upper crust is 25 km and that of the lower crust 20 km. The mantle rheology is that for olivine. A large-scale thrust fault dipping to the west with an angle of 35° separates two crustal blocks. For the calculations, the mantle region has a thickness of 70 km. This value corresponds to the depth to the 700–750°C isotherm, for which the continental mantle can no longer sustain deformations over geological time-scales (see [10]).

3.5. Numerical methods

In order to predict topography and Moho variations induced by crustal loads, we have used two numerical schemes which allow for complicated geometrical structures and non-linear mechanical properties (plastic–elastic–viscous rheology with non-Newtonian ductile creep viscosity).

The first 2D finite-element scheme used in this study was developed from the finite element code TECTON [36] and the second, PARAVOZ [37,38], is based on the Fast Lagrangian Analysis of Continua (FLAC) algorithm [39] (see Appendix A). A summary of the algorithms used and of the assumed rheology models is given in Table 4. The classical elastic thin plate model was used along with the finite element models to check the compatibility of the *internal* EET predicted by these different models. The results of the numerical experiments are interpreted in terms of the effective elastic thickness as defined in Appendix A.

Numerical methods, such as the FE and FLAC methods, require interpretation of the results. Approximate methods provide a more straightforward interpretation of the physics involved, and we have also used a semi-analytical inelastic plate model developed in [40,10] to compare with the pure numerical methods.

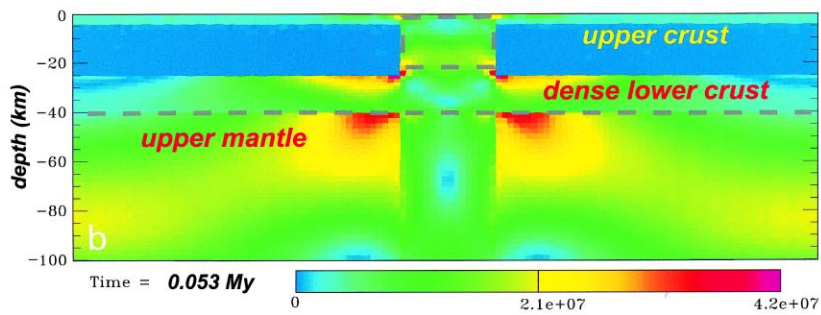
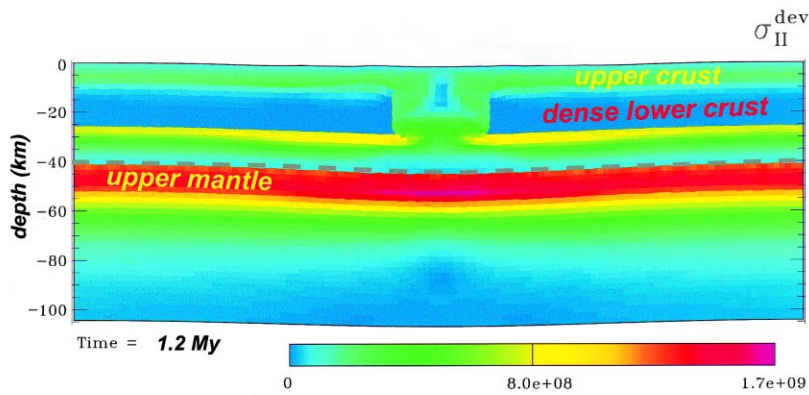
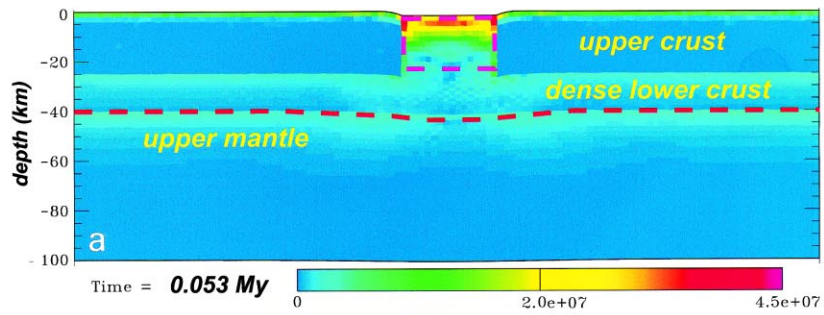
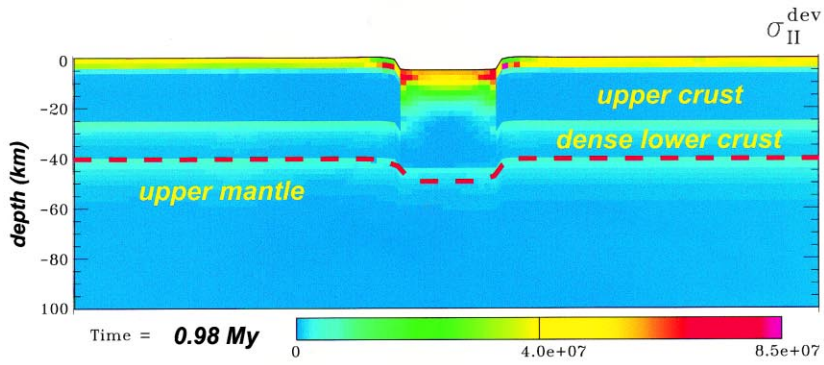


Table 4
Rheological parameters and algorithms used in the numerical models

Model	Algorithm	Upper crust rheology	Lower crust rheology	Mantle rheology	Thermal model
Fig. 3	Burov and Diament	elastic	elastic	elastic	n.a.
Fig. 6a	Paravoz	quartz (weak) ^a	diorite (weak) ^a	olivine (weak) ^a	'hot' ^c
Fig. 6b	Paravoz	quartz (strong) ^b	diorite (strong) ^b	olivine (strong) ^b	'cold' ^c
Fig. 7a	Paravoz, Tecton	quartz (strong) ^a	diorite (strong) ^a	olivine (strong) ^a	'cold' ^c
Fig. 7b	Paravoz, Tecton	quartz (strong) ^b	diorite (strong) ^b	olivine (strong) ^b	'cold' ^c
Fig. 8	Tecton	quartz (strong) ^b	diorite (strong) ^b	olivine (strong) ^b	'cold' ^c
Fig. 9	Tecton	quartz (strong) ^b	diorite (strong) ^b	olivine (strong) ^b	'cold' ^c

^a First value in Table 1.

^b Second value in Table 1.

^c See Table 3.

The parameters are taken such that the depth integrated strength fits the EET values: 30 km for the weak rheology and 90 km for the strong rheology.

4. Results

4.1. Effect of the internal load

To separate the effects of the fault from those of the dense crustal block, we made a first set of calculations without a fault (Fig. 5). The dense crustal block lies in the upper crust: it is 25 km thick and 40 km wide. These dimensions and volume are on the same order as those of the Kapuskasing structure. The density contrast, fixed at 250 kg m^{-3} , corresponds to the difference between the upper crust and the denser granulites. These values are standard for the region [28] and are consistent with the Bouguer anomaly. Without lower crustal flow, isostatic subsidence would be 9.9 km. These calculations were done with the algorithm PARAVOZ with two different sets of rheological and thermal parameters that are given in Tables 1 and 2. Fig. 5a shows the resulting stress and strain fields after 1 and 3 m.y. using the rheology implied by the continental geotherm of [6] with the 800°C isotherm at 100 km. In this case with a weak rheology, the dense crustal block is capable of producing a large-scale elastic bending of the lithosphere only at the initial stage of deformation, but then it sinks in the mantle in a few million years creating a deep narrow basin on the

surface. This is clearly inconsistent with the observations which suggest that the block should stay near the upper surface. Fig. 5b illustrates the behaviour of a significantly stronger plate, corresponding to the 'cold' thermal structure of Jaupart et al. [30]. The induced surface deformation is smaller and flexural in nature, as the plate bends slightly under the load. For this choice of parameters, the plate deflection of 7 km is close to the observed crustal thickening beneath Kapuskasing. This structure is not in a local isostatic equilibrium and is supported by the strength of the lithosphere on a regional scale.

Many workers have correlated, by analogy with the oceans, the continental EET with the depth to the $450\text{--}550^\circ\text{C}$ isotherm, but the strong part of the continental lithosphere should extend to a greater depth for several reasons. At a given pressure, the rheology is stronger when the temperature is lower. The colder the geotherm, the higher is the pressure corresponding to the same temperature. The activation enthalpy increases with depth, implying pressure hardening following the olivine flow law of Table 1. The latter effect leads to $\approx 150^\circ\text{C}$ increase in the temperature of ductile yielding. In cratons, the background tectonic strain rates are typically one–two orders lower than those in younger tectonically active areas resulting in higher viscosity at the same temperature

Fig. 5. (a) Stress (second invariant of shear stress, Pa) caused by a dense inclusion (2950 kg m^{-3}) in the upper crust. These calculations are for the weakest rheology from Table 1 with 'hot' lithospheric geotherm [6]. The sediment fill is not shown. Two stages are shown: initial (bottom) and developed (top). (b) Same calculation as in (a) for stronger rheology (Table 1) and cold geotherm from [30] (see Fig. 4).

(power law materials have higher viscosities at lower strain rates, Table 1). Very recent experiments on the strength of lower crustal materials (diabase) at high temperature [41] suggest that dry diabase may maintain a very high strength (>2 GPa) at 500° – 600° C and stay remarkably strong up to 700° C. However, for very weak lower crustal compositions and young lithosphere (<700 Ma), the EET can be significantly reduced by mechanical decoupling between the upper crust and upper mantle [10]. However, this has no effect on the depth to the bottom of the strong mantle which stays fixed at around 700 – 750° C.

4.2. Effect of the internal load with thrust fault

The geometry of this model is shown in Fig. 6. For these calculations, we have used the parameters corresponding to the strong rheology (Table 1).

The coefficient of friction and the dip of the fault were varied. These calculations were performed and cross-checked using both algorithms TECTON and PARAVOZ.

Model results are presented in Fig. 7. These calculations are carried out for a strong rheology, corresponding to our working model for the lithosphere. With slip allowed on the fault in the absence of strong counteracting tectonic compression, the deformation is concentrated along the fault plane (Fig. 7a) and leads to important surface subsidence. At Kapuskasing, the fault is ancient and likely to be healed and to not allow slip. In this case, the deformation is small and symmetrical about the centre of the anomalous crustal structure (Fig. 7b). The plate reaction in this case is predominantly large-scale bending with maximum amplitude beneath the fault. Fig. 8 shows the local strength integrated from the

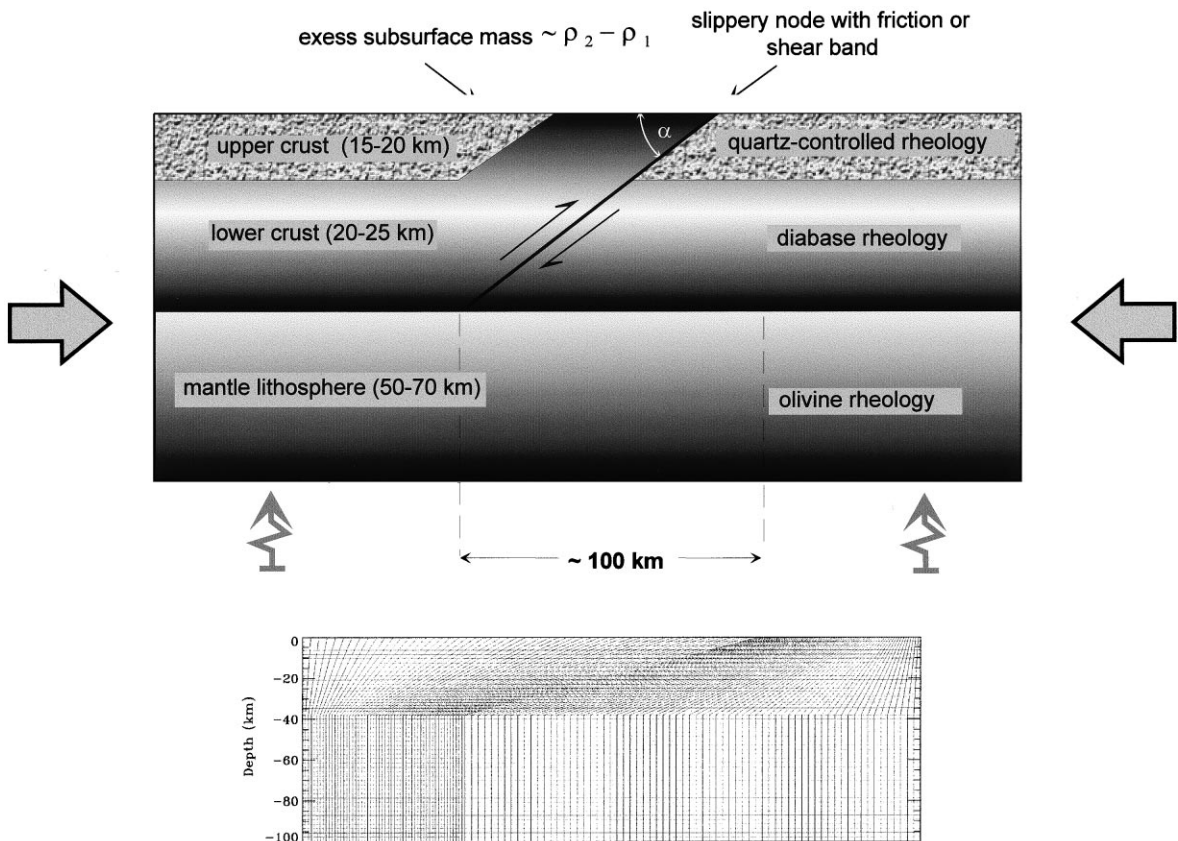


Fig. 6. Sketch of the geometry of the layered elasto-viscous plate model assuming rheological heterogeneities associated with the ancient fault and the geometry of the finite element mesh.

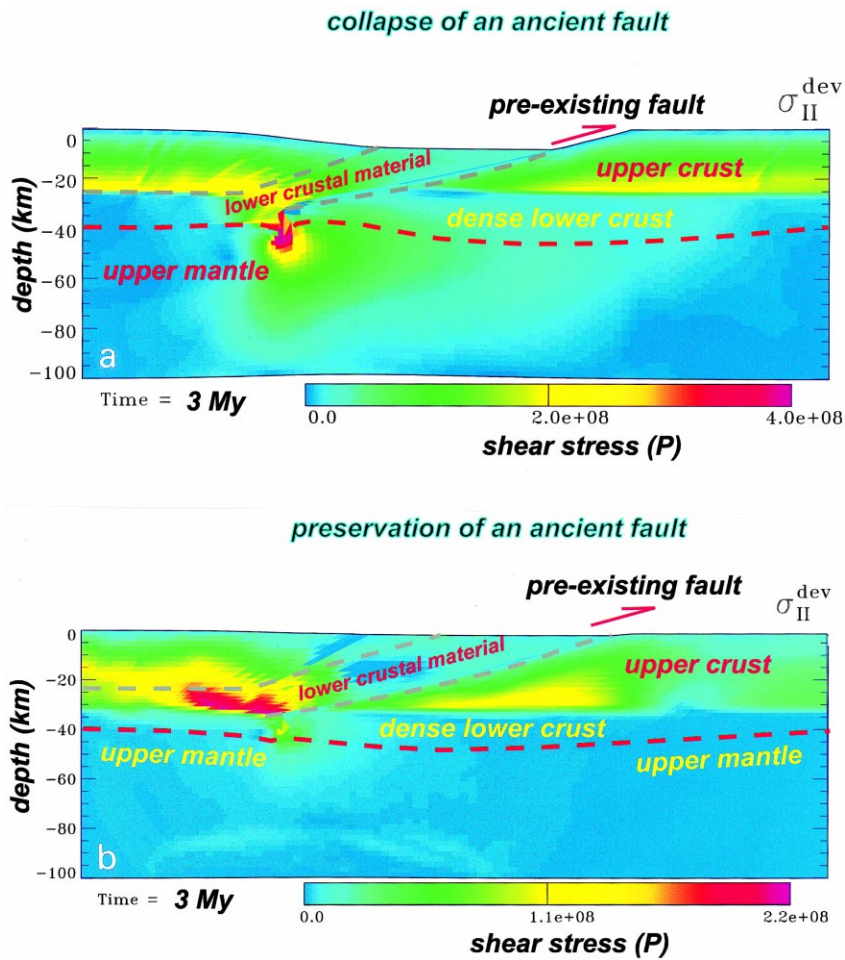


Fig. 7. (a) Displacements and stress distributions (second invariant of shear stress, Pa) associated with high-density inclusion and non-healed thrust fault (friction angle of the plastic part $\beta = 30$, cohesion $\sigma_0 = 20$ MPa, $k = 0.55$, cohesion strain softening at strains greater than 0.1). (b) Same with healed thrust fault.

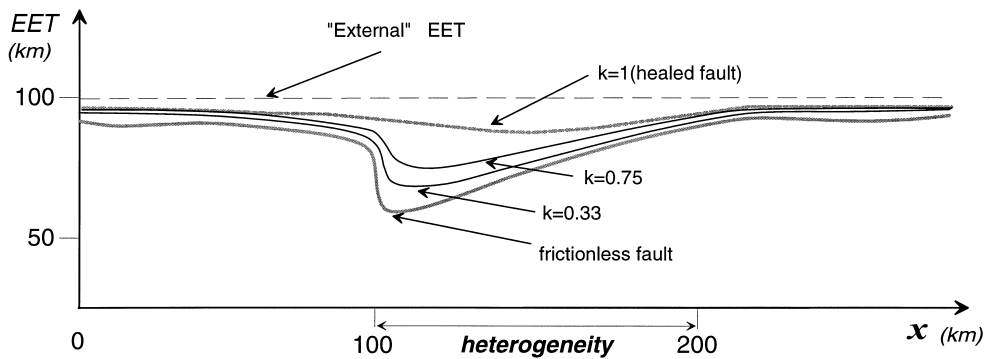


Fig. 8. Integrated lithospheric strength (EET) variations for different Amonton/Anderson's frictional coefficients (k) on the fault. $k = 1$ means completely healed fault, $k = 0$ is for frictionless fault. At $k = 1$ the lithosphere is still weakened due to inelastic yielding under flexural stresses caused by the high-density subsurface load.

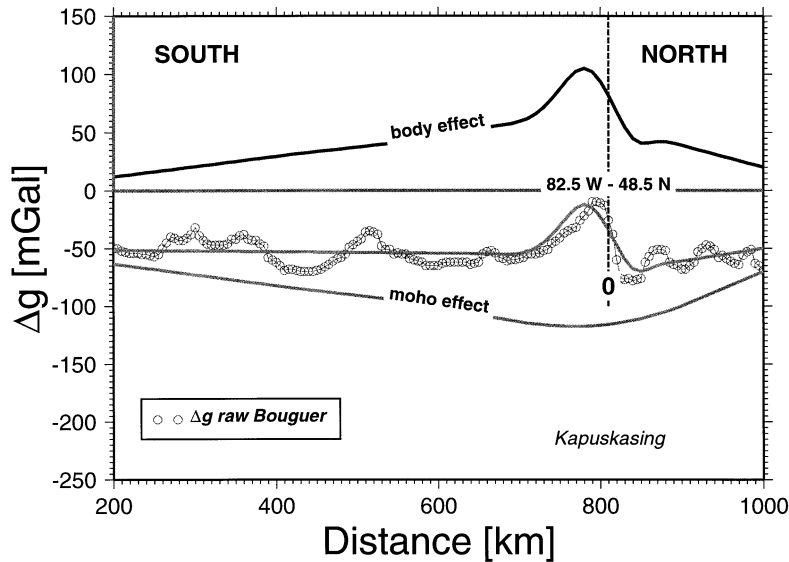


Fig. 9. Gravity anomaly for a dense granulite body and plate flexure beneath the Kapuskasing uplift: anomaly due to the subsurface granulite body only (upper solid curve), anomaly due to the related Moho depression (lower curve), and the resulting gravity anomaly (central curve).

results of stress/strain rate calculations with different friction coefficients (Appendix A). These results support our assumption that the thrust fault should be healed. If it were not so, it would require constant tectonic compression for 2 Ga to prevent large-scale subsidence. To ensure that equilibrium is reached, calculations were performed for a total duration of 30 Ma, and the final results are presented as local values of the elastic thickness as defined in Appendix A (Fig. 8). It is noteworthy that the strength reduction occurs where 'strong' lower crustal rocks are emplaced in the upper crust. The non-linear rheology implies that the plate is locally weakened by the flexural stresses induced by the dense body. The plate remains strong away from this body (Fig. 8), so that the effective elastic thickness can vary horizontally from <70 km to 100 km. The EET remains larger than the values inferred by extrapolating the oceanic EET-age-temperature relationship. Fig. 9 shows the calculated gravity anomalies for the cold continental geotherm and the crustal model of Fig. 7. Using 'dry' rheological parameters (Table 1), we obtain a good fit to the gravity profile across the Kapuskasing structure. The long-wavelength increase in Bouguer anomaly due to the load is compensated by the Moho deflection. The asymmetrical gravity anomaly is due

to the sum of two effects: the topography of the Moho and the dense crustal block.

Our results suggest that special boundary conditions must have prevailed to permit the stabilization of the heterogeneities at 2 Ga, when the lithosphere was weaker because of higher crustal heat generation and a non-healed fault. The large load due to the thrusting of lower crustal rocks would induce a large plate flexure if the elastic thickness was small, because of high temperatures in the mantle part of the lithosphere. One could calculate the stresses required to generate the Kapuskasing structure, but this is beyond the scope of this paper.

5. Conclusions

In this study, we have examined the present conditions for the preservation of density heterogeneities and crustal roots in cratons. Our results show that a crustal root can be maintained in old cratons only if the crustal and mantle rheologies include a very strong ductile part. This conclusion is consistent with the thermal model derived from the heat flow data [28,30] and commonly inferred values of the experimental rheological parameters. In this case, because

of the high effective viscosity or/and of the plastic (brittle) behaviour, the load is not sufficient to activate significant ductile/viscous deformation. Alternatively, a compressional stress regime or some very well *adopted* subsurface processes would be required to prevent the collapse of such large crustal structures.

Large-scale variations of EET result not only from lateral changes in the rheological properties of the crust but also from the non-linearity of the rheology. Away from the Kapuskasing structure, the EET is about 100 km, as suggested for the centre of the Canadian Shield [1,2]. The EET is minimum at the ancient healed fault zone. Direct application of *admittance* methods to the Kapuskasing area would have yielded different results. The lithospheric strength in the Kaspuskasing zone can be lower than indicated by the EET estimated from Bouguer anomalies, but significantly higher than the values that could be obtained from free-air anomalies. Our results suggest that standard methods for estimating the EET (admittance, coherence) must be applied with care in old cratonic areas. In such areas, the signal-to-noise ratio is too low to distinguish between the gravity anomalies due to plate deflection induced by surface loads and anomalies due to the lateral heterogeneities. Wherever surface topography and subsurface loads do not provide the dominant contribution to the plate deformation, tectonic forces must be included. In such areas, forward mechanical modelling is more appropriate than EET to study the rheological structure of the lithosphere. This conclusion is equally applicable to the young lithosphere in zones of active deformation where the tectonic boundary forces are important and may provide the same contribution to the plate deflection as the topography.

Our experiments demonstrate that a weak lithosphere (EET <50–70 km) is unlikely in cratons. In absence of tectonic forces, the persistence of dense crustal blocks requires high lithospheric strength, with a strong diabase-like lower crust (i.e., effective viscosity at the brittle–ductile transition >10²⁷ Pa s). Our modelling shows that during deformation, a large portion of the strong mantle lithosphere may stay competent. Strong mantle and lower crust are needed to support dense crustal inhomogeneities, implying that old continental material only yields

at high temperatures. Yield temperatures of 450° or even 600°C, which have been proposed by analogy with the oceanic lithosphere, seem inconsistent with the structure of cratons.

Acknowledgements

E. Burov has greatly benefited from discussions with A.B. Watts, C. Ebinger and P. Molnar. The finite element code TECTON used with some modifications in this study was kindly provided by J. Melosh. The algorithm PARAVOZ originates from A. Poliakov (and Y. Podladchikov), who is deeply thanked for driving attention to this method, enthusiastic help, and many useful discussions. Some figures were done with the public domain graphics package GMT by Wessel and Smith. The authors appreciate very constructive reviews by Greg Houseman and an anonymous reviewer. This is BRGM publication number 98024. J.-C. Mareschal is grateful for the constant support of the natural sciences and engineering research council (Canada). This is Lithoprobe publication 955. [AC]

Appendix A. Effective elastic thickness of inelastic lithosphere

The conservation Eq. 1 has been solved numerically with two different algorithms. The PARAVOZ code is the fully explicit time-marching algorithm analogous to the FLAC algorithm [39] that solves the full equations of motion:

$$\rho \frac{\partial v}{\partial t} + \nabla \cdot \sigma - \rho g = 0 \quad (\text{A1})$$

Solution of the equations provide velocities at mesh points which are used to calculate element strains. These strains are used in the constitutive relations to calculate element stresses and equivalent forces which form the basic input for the next calculation cycle.

To solve explicitly the governing equations, the FLAC method uses a dynamic relaxation technique by introducing artificial masses in the inertial system. An adaptive remeshing technique permits to resolve strain localizations leading to the formation of faults. The solver of the FLAC method does not require any rheology assumption in contrast to most finite element techniques based on the displacement method that requires forming new elements for each new rheology. Because of this FLAC feature, any constitutive law is easily introduced in the numerical scheme. Another advantage of this method is that it does not require the inversion of large stiffness matrices. Because it is memory efficient, the algorithm permits better resolution than traditional FEM codes.

The EET of a plate of arbitrary rheology is determined by the semi-analytical inelastic plate approximation algorithm [10]. This algorithm calculates the EET from the stress distribution. This algorithm first computes the effective bending moment M_x , the longitudinal and vertical components of the force T_x and Q_x , respectively

$$M_x = - \int_0^\infty \sigma_{xx}(z - z_n) dz \quad (A2)$$

$$T_x = - \int_0^\infty \sigma_{xx} dz \quad (A3)$$

$$Q_x = - \int_0^\infty \sigma_{xz} dz \quad (A4)$$

where z is depth, and z_n is the depth to the neutral plane (which are tracked during computations). The EET is determined from:

$$-\frac{\partial^2 M_x}{\partial x^2} + \frac{\partial}{\partial x} \left(T_x \frac{\partial w}{\partial x} \right) + p_- = p_+ \quad (A5)$$

$$T_e = \left(\frac{D(\Phi)}{D_0} \right)^{1/3} = \left(\frac{-M_x(\Phi) R_{xz}}{D_0} \right)^{1/3} \\ = \left(\frac{M_x(\Phi)}{D_0} \left(\frac{\partial^2 w}{\partial x^2} \right)^{-1} \right)^{1/3} \quad (A6)$$

where w is the vertical deflection of the plate, p_- is the buoyancy force per unit area, p_+ is the sum of the surface and internal loads, $D_0 = E/(12(1 - \nu^2))$, E and ν are Young's modulus and Poisson's ratio, respectively, $R_{xz} \approx -1/w''$ is the observed radius of plate curvature.

For several layers with distinct rheological properties, the effective rigidity D is calculated from the vertical gradient of bending stress. The bending stress is determined by the second derivative of plate deflection w (or radius of flexure R_{xy}):

$$D(\Phi) \frac{\partial^2 w}{\partial x^2} = - \frac{D(\Phi)}{R_{xy}} = -M_x(\Phi) \quad (A7)$$

where $M_x(\Phi)$ is the effective bending moment which can be estimated directly as:

$$M_x = - \sum_{i=1}^N \sum_{j=1}^{M_i} \int_{z_{ij}^-}^{z_{ij}^+} \sigma_{xx}^j(x, z) z_i^*(x) dz \quad (A8)$$

where N is the number of mechanically detached rheological layers of variable thickness $z_i^* = z - z_{ni}(x)$, z_{ni} is the depth to the i th neutral plane; z_{ij}^+ and z_{ij}^- are the respective depths to the lower and upper low-strength. Correspondingly, the thickness of the i th detached layer is $z_{ij}^+ - z_{ij}^-$. The parameter M_i is the number of 'welded' (continuous) elastic, ductile or brittle layers in the i th detached layer: $\sigma_{xx}^j(x, z) = \sigma(\epsilon)$ is the bending stress defined for material parameters of j sub-layer belonging to the i detached layer, $j = j(i)$. The thickness of the 'welded' layers is not constant but is determined by local stress, strain rate and temperature.

References

- [1] D. Bechtel, D.W. Forsyth, V.L. Sharpton, R.A.F. Grieve, Variations in effective elastic thickness of the North American lithosphere, *Nature* 343 (1990) 636–638.
- [2] M. Pilkington, Mapping elastic lithospheric thickness variations in Canada, *Tectonophysics* 190 (1991) 283–287.
- [3] D.W. Forsyth, Subsurface loading and estimates of the flexural rigidity of continental lithosphere, *J. Geophys. Res.* 90 (1985) 12623–12632.
- [4] M.T. Zuber, T.D., Bechtel, D.W. Forsyth, Effective elastic thickness of the lithosphere and mechanisms of isostatic compensation in Australia, *J. Geophys. Res.* 94 (1989) 9353–9367.
- [5] R.W. Hartley, A.B. Watts, J.D. Fairhead, Isostasy of Africa, *Earth Planet. Sci. Lett.* 137 (1996) 1–18.
- [6] D.P. McKenzie, D. Fairhead, Estimates of the effective elastic thickness of the continental lithosphere from Bouguer and free air gravity anomalies, *J. Geophys. Res.* 102 (1997) 27523–27552.
- [7] A.R. Lowry, R.B. Smith, Flexural rigidity of the Basin and Range — Colorado Plateau–Rocky Mountain transition from coherence analysis of gravity and topography, *J. Geophys. Res.* 99 (1994) 20123–20140.
- [8] A. Macario, A. Malinverno, W.F. Haxby, On the robustness of elastic thickness estimates obtained using the coherence method, *J. Geophys. Res.* 100 (1995) 15163–15172.
- [9] J.C. Mareschal, J. Kuang, Intraplate stresses and seismicity: the role of topography and density heterogeneities, *Tectonophysics* 132 (1986) 153–162.
- [10] E.B. Burov, M. Diament, The effective elastic thickness (T_e) of continental lithosphere: what does it really mean?, *J. Geophys. Res.* 100 (1995) 3905–3927.
- [11] A.B. Watts, J.H. Bodine, N.M. Ribe, Observations of flexure and geological evolution of the Pacific Ocean basin, *Nature* 283 (1980) 532–537.
- [12] A.V. Boland, R.M. Ellis, Velocity structure of the Kapuskasing uplift, northern Ontario, from seismic refraction studies, *J. Geophys. Res.* 94 (1989) 7189–7204.
- [13] J.A. Percival, G.F. West, The Kapuskasing uplift: a geological and geophysical synthesis, *Can. J. Earth Sci.* 31 (1994) 1256–1286.
- [14] J.A. Percival, K.D. Card, Archean crust as revealed in the Kapuskasing uplift, Superior Province, Canada, *Geology* 11 (1983) 323–326.
- [15] J.A. Percival, P.H. McGrath, Deep crustal structure and tectonic history of the northern Kapuskasing uplift of Ontario: an integrated petrophysical–geophysical study, *Tectonics* 5 (1986) 553–572.
- [16] H.C. Halls, H.C. Palmer, M.P. Bates, W.C. Phinney, Constraints on the nature of the Kapuskasing zone from the study of Proterozoic dike swarms, *Can. J. Earth Sci.* 31 (1994) 1182–1196.
- [17] W.T. Geis, F.A. Cook, A.G. Green, J.A. Percival, G.F. West, B. Milkereit, Thin thrust sheet formation of the Kapuskasing structural zone revealed by Lithoprobe seismic reflection data, *Geology* 18 (1990) 513–516.

- [18] J.J. Wu, R.F. Mereu, The nature of the Kapuskasing structural zone: results from the 1984 seismic refraction experiment, in: M.H. Salisbury, D.M. Fountain (Eds.), *Exposed Cross Sections of the Continental Crust*, Kluwer, Dordrecht, 1990, pp. 563–586.
- [19] A.V. Boland, R.M. Ellis, A geophysical model for the Kapuskasing uplift from seismic and gravity studies, *Can. J. Earth Sci.* 28 (1991) 342–354.
- [20] J.J. Wu, R.F. Mereu, Crustal structure of the Kapuskasing uplift from Lithoprobe near-vertical/wide angle seismic reflection data, *J. Geophys. Res.* 97 (1992) 17442–17453.
- [21] E.A. Atekwana, M.H. Salisbury, J. Verhoef, N. Culshaw, Ramp-flat geometry within the central Kapuskasing uplift? Evidence from potential field modeling results, *Can. J. Earth Sci.* 31 (1994) 1027–1041.
- [22] O.I. Parphenuk, V. Dechoux, J.C. Mareschal, A finite element model of formation for the Kapuskasing structural zone, *Can. J. Earth Sci.* 31 (1994) 1227–1234.
- [23] J. Gratton, Crustal shortening, root spreading, isostasy, and the growth of orogenic belts: a dimensional analysis, *J. Geophys. Res.* 94 (1989) 15627–15634.
- [24] P. Bird, Lateral extrusion of lower crust from under high topography in the isostatic limit, *J. Geophys. Res.* 96 (1991) 10275–10286.
- [25] J.P. Avouac, E.B. Burov, Erosion as a driving mechanism of intracontinental mountain growth?, *J. Geophys. Res.* 101 (1996) 17747–17769.
- [26] J.C. Mareschal, C. Pinet, C. Gariépy, C. Jaupart, G. Bienfait, G. Dalla-Coletta, J. Jolivet, R. Lapointe, New heat flow density and radiogenic heat production data in the Canadian Shield and the Québec Appalachians, *Can. J. Earth Sci.* 26 (1989) 825–852.
- [27] C. Pinet, C. Jaupart, J.C. Mareschal, C. Gariépy, G. Bienfait, R. Lapointe, Heat flow and lithosphere structure of the eastern Canadian Shield, *J. Geophys. Res.* 96 (1991) 19923–19941.
- [28] L. Guillou-Frottier, J.C. Mareschal, C. Jaupart, C. Gariépy, R. Lapointe, G. Bienfait, Heat flow variations in the Grenville Province, Canada, *Earth Planet. Sci. Lett.* 136 (1995) 447–460.
- [29] L. Guillou-Frottier, C. Jaupart, J.-C. Mareschal, C. Gariépy, G. Bienfait, L.Z. Cheng, R. Lapointe, *Geophys. Res. Lett.* 23 (1996) 3027–3030.
- [30] C. Jaupart, J.C. Mareschal, L. Guillou-Frottier, A. Davaille, Heat flow and thickness of the lithosphere in the Canadian Shield, *J. Geophys. Res.* 103 (1998) 15269–15288.
- [31] W.F. Brace, D.L. Kohlstedt, Limits on lithospheric stress imposed by laboratory experiments, *J. Geophys. Res.* 85 (1980) 6248–6252.
- [32] N.L. Carter, M.C. Tsenn, Flow properties of continental lithosphere, *Tectonophysics* 136 (1987) 27–63.
- [33] G. Ranalli, D.C. Murphy, Rheological stratification of the lithosphere, *Tectonophysics* 132 (1987) 281–295.
- [34] Ranalli, G., *Rheology of the Earth*, Chapman Hall, London, 1995, 2nd ed., 413 pp.
- [35] J.D. Byerlee, Friction of rocks, *Pure Appl. Geophys.* 116 (1978) 615–626.
- [36] H.J. Melosh, Mechanical basis for low-angle normal faulting in the Basin and Range province, *Nature* 343 (1990) 331–335.
- [37] A.N.B. Poliakov, P. Cundall, Y. Podladchikov, V. Laykhovskiy, An explicit inertial method for the simulation of viscoelastic flow: an evaluation of elastic effects on diapiric flow in two- and three-layers models, in: D.B. Stone, S.K. Runcorn (Eds.), *Flow and Creep in the Solar System: Observations, Modeling and Theory, Dynamic Modelling and Flow in the Earth and Planets*, Kluwer, Dordrecht, 1993, pp. 175–195.
- [38] A.N.B. Poliakov, Yu. Podladchikov, C. Talbot, Initiation of salt diapirs with frictional overburden: numerical experiments, *Tectonophysics* 228 (1993) 199–210.
- [39] P.A. Cundall, Numerical experiments on localization in frictional materials, *Ingenieur Arch.* 59 (1989) 148–159.
- [40] E.B. Burov, M. Diament, Flexure of the continental lithosphere with multilayered rheology, *Geophys. J. Int.* 109 (1992) 449–468.
- [41] S.J. Mackwell, M.E. Zimmerman, D.L. Kohlstedt, High-temperature deformation of dry diabase with application to tectonics on Venus, *J. Geophys. Res.* 103 (1998) 975–984.